Research Paper

Numerical investigation on multi-stage swirl cooling at mid-chord region of gas turbine blades

Yongle Ma [a,b,c], Xuejun Fan [c,d], Xiulan Huai [a,b,c], Keyong Cheng [a,b,c,*]

[a] Institute of Engineering Thermophysics, Chinese Academy of Sciences, Beijing 100190, China
[b] Nanjing Institute of Future Energy System, Nanjing 210000, China
[c] School of Engineering Science, University of Chinese Academy of Sciences, Beijing 101408, China
[d] Institute of Mechanics, Chinese Academy of Sciences, Beijing 100190, China

ABSTRACT

Compared with the single-stage one, the multi-stage swirl cooling technique has great potential at the mid-chord region of gas turbine blades. Currently, the effect of the chamber structure at the mid-chord region of the blades on the multi-stage swirl cooling is still unknown. In this study, four kinds of the multi-stage swirl chamber models are built: Case 1 has two swirl nozzles and three chambers, and cases 2–4 have six swirl nozzles and seven chambers. Fluid flow and heat transfer characteristics of the coolant in the swirl cooling configurations are numerically investigated. The standard *k-ε* turbulent model is adopted in current study and the Reynolds number of the coolant varies from 12,000 to 52000. The results show that the long swirl chamber in case 1 has negative effect on the performance of the swirl cooling this is because the swirl velocity along the axial direction is gradually reduced and the Nusselt number is decreased remarkably. For cases 2–4, the chambers are separated into several short ones. Therefore, the swirl velocity could keep high value and so is the Nusselt number. Although more swirl chambers could lead to higher pressure loss coefficient, cases 2–4 show better comprehensive thermal performance as compared to case 1. Among the current cases, the swirl chamber structure in case 4 shows the highest cooling effectiveness and obtains more uniform temperature distributions on the external surface of the blade.

1. Introduction

Nowadays, gas turbines have been widely used in aviation, industrial power generation, ship power, and other areas. The turbine inlet temperature (TIT) affects the thermal efficiency and power output of gas turbines and is enhanced continuously year by year. At present, the TIT of the industrial gas turbines is higher than 1700 K, which is far beyond the melt point of the blade materials [1]. Therefore, the cooling techniques, such as film cooling, impingement cooling, enhanced convective heat transfer and so on, are extensively adopted to protect the safe operation of turbine blades. Among them, swirl cooling is an efficient cooling technique which could introduce the coolant through the jet nozzle to produce vortex flow. Kreith et al. [2] and Hay et al. [3] pointed out that the heat transfer capability of swirl flow is at least four times higher than that of the flow without swirl. This technique could not only show the high comprehensive thermal performance without increasing the mass flow rate of the cooling air, but also achieve uniform

temperature distributions, and has become a hot research topic in the field of gas turbine blade cooling [4].

Currently, swirl cooling is mainly adopted at the leading edge region of gas turbine blades and related experimental studies have been conducted. For example, Glezer et al. [5] investigated the performance of swirl cooling and the results demonstrate that swirl cooling could show comparable or better performance as compared to the impingement cooling or impingement and film compound cooling. After that, Hedlund et al. [6,7] analyzed the development of Gortler vortex pairs in a concave chamber with swirl flow through the flow visualization experiments. Biegger et al. [8,9] studied the inlet and outlet geometries on the swirl cooling performance. The results show that more uniform heat transfer could be achieved by the swirl chamber with multiple inlets at the price of lower pressure loss. Fan et al. [10,11] presented the effects of Reynolds number and temperature ratio on the flow and heat transfer characteristics of swirl cooling. In recent years, numerical studies on swirl cooling of the gas turbine blade leading edge are gradually increased. Fawzy et al. [12,13], Mousavi et al. [14], and Fan et al.

Nomenclature

A_a	Cross-sectional area of the chamber, m^2
C_{Pt}	Pressure loss coefficient
D	Average hydraulic diameter of the cooling chambers, m
f	Friction factor
f_∞	Friction factor of the smooth tube
$\dot{I}_\varphi$	Averaged angular momentum, kg·m/s
$\dot{I}_z$	Averaged axial momentum, kg·m/s
j	Comprehensive thermal performance
L	Length, m
$\dot{m}$	Mass flow rate, kg/s
Nu	Nusselt number
Nu_∞	Nusselt number of the smooth tube
P	Local pressure of the coolant, Pa
ΔP	Pressure difference, Pa
Pr	Prandtl Number
q	Average heat flux at the interface between the fluid and solid region, J/(m^2•K)
R	Radius, m
Re	Reynolds number
S	Circumferentially averaged swirl number

T	Temperature, K
T_b	Coolant temperature, K
T_{wi}	Wall temperature, K
T_h	Mainstream inlet temperature, K
T_c	Coolant inlet temperature, K
T_{wo}	External wall temperature of the blade, K
U	Velocity, m/s
u_φ	Circumferential velocity, m/s
u_z	Axial velocity, m/s

Greek symbols

ρ	Density, kg/m^3
λ	Thermal conductivity of the coolant, W/(m·K)
μ	Dynamic viscosity, Pa·s
η	Cooling effectiveness
σ	Non-uniformity factor of the temperature

Subscripts

in	Inlet
ave	Averaged
P	Pressure surface
S	Suction surface

[15,16] investigated the effects of inlet nozzle structures, such as nozzle area, inject angle, nozzle location and so on, and gave the reasonable suggestions for the leading edge cooling of gas turbine blades under different Reynolds numbers. The swirl chamber is also a key research point and Wang et al. [17] investigated the effect of the cross-sectional areas of swirl chambers and concluded that the swirl chamber shows a higher heat transfer performance and a lower aerodynamic loss when the draft angle is above 0°. Li et al. [18] studied the effect of chamber heights on the performance of the swirl cooling and the proper chamber heights are suggested according to the different operation conditions of gas turbines. Liu et al. [19] adopted the dimpled swirl chamber instead of the common smooth one. The results show that the heat transfer and pressure drop are increased by 7.2 % and reduced by 17.6 % because the dimples increase the heat transfer area of the swirl chamber. Alhajeri

(a) Top view

(b) Side view

Fig. 1. Geometry model.

et al. [20] demonstrated flow and heat transfer characteristics of the coolant in a ribbed chamber. They concludes that the swirl cooling could achieve better performance in a ribbed chamber when the Reynolds number is lower than 500000. Besides the above research, the combined effect of swirl cooling and film cooling is also attracted attention [21,22]. For example, Wang et al. [23] and Zhou et al. [24] explored the combined effect of swirl cooling and effusion cooling and compared with the impingement/effusion cooling method, the swirl/effusion cooling method shows more uniform coolant distribution. Wang et al. [25] studied the effect of coolant injection direction on the swirl/film compound cooling and flow and heat transfer characteristics of the coolant are analyzed due to the interaction of the mainstream and swirl flow. The above mentioned cooling method, which employs one swirl chamber and several inlet nozzles, is called the single-stage swirl cooling. The drawback of this structure is that the cooling capability of the coolant along the flow direction in the swirl chamber is reduced gradually due to the viscous effect and swirl flow decay. Therefore, Yao et al. [26] proposed the multi-stage swirl cooling for which the swirl chamber has been divided into several stages. The results show that compared with the single-stage one, the multi-stage swirl cooling could not only achieve higher heat transfer capability and pressure drops, but also obtain more uniform temperature distributions. However, the pressure drops in the multi-stage swirl chambers are reduced remarkably through optimizing the connection region of adjacent chambers.

Although the thermal load at the mid-chord region of the blade is not as high as that at the leading edge, the cooling of this part is of equal importance and various methods, such as enhanced convective heat transfer with ribs, impingement cooling, alternating elliptical channels, and so on, have been investigated thoroughly [27–30]. The room for further improving the performance of these techniques is limit. Therefore, considering its comparatively high and uniform cooling capability, the swirl cooling method has been tried to be employed at the mid-chord region of the blade. Bruschewski et al. [31,32] analyzed flow characteristics of swirl cooling in a U-shaped channel. The results show that the 180-deg bend reduces the tangential velocity of the coolant and therefore the heat transfer capability is decreased. Khalatov et al. [33] investigated the two-stage swirl cooling in three channels of a turbine blade. The results show that the heat transfer performance is enhanced with acceptable aerodynamic loss in two swirl chambers. Friction factor and Nusselt number correlations are concluded based on the
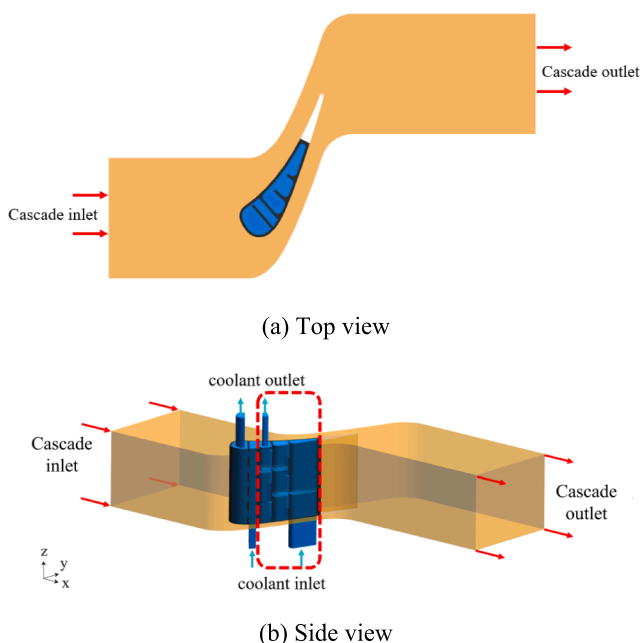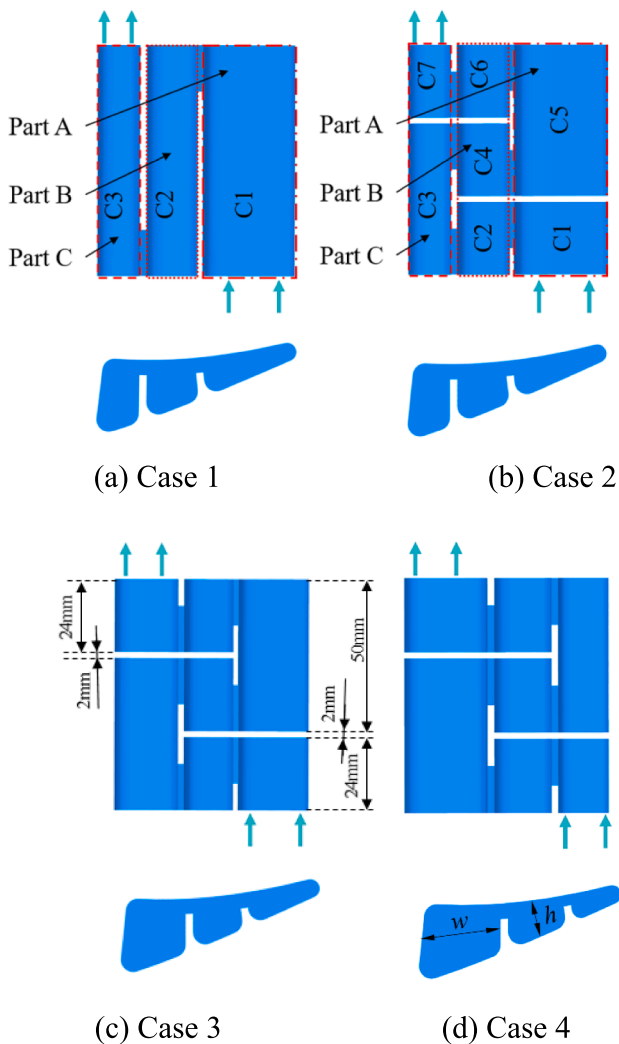
(a) Case 1   (b) Case 2

(c) Case 3   (d) Case 4

Fig. 2. The swirl cooling structure at the mid-chord region.

Table 1
The cross-sectional area of each part.

Part	Case 1	Case 2	Case 3	Case 4
A	A_a: 265.5 mm^2	A_a: 265.5 mm^2	A_a: 181.9 mm^2	A_a: 111.7 mm^2
	AR: 3.69	AR: 3.69	AR: 3.25	AR: 2.46
B	A_a: 257.7 mm^2	A_a: 257.7 mm^2	A_a: 210.8 mm^2	A_a: 209.9 mm^2
	AR: 1.08	AR: 1.08	AR: 1.23	AR: 1.61
C	283.1 mm^2	A_a: 283.1 mm^2	A_a: 424.6 mm^2	A_a: 509.2 mm^2
	AR: 0.59	AR: 0.59	AR: 0.98	AR: 1.28

leading-edge region and the mid-chord region. Although the main research part is the mid-chord region in this study, the single-stage swirl cooling with five inlet nozzles is still adopted in the leading edge to reduce the temperature gradient between the leading edge and mid-chord region. The length and width of the inlet nozzles are 5 mm and 1.5 mm, respectively. The heights of the inlet chamber and the swirl chamber are 8 mm and 19 mm, respectively. This cooling structure shows the best performance according to the results conducted by Li et al. [18]. As shown in Fig. 2, the mid-chord region is divided into three parts (Part A, B, and C) and each part in case 1 has one chamber. For example, part A includes chamber 1 (C1), and part B includes chamber 2 (*C*2), and part C includes chamber 3 (C3). In case 2, the cross-sectional area of each part is the same as that in case 1. However, each part is separated into two or three chambers through the swirl nozzles. For example, part A includes chambers 1 and 5 (C1, C5), and part B includes chambers 2, 4, 6 (C2, C4, and C6), and part C includes chambers 3 and 7 (C3 and C7). In order to investigate the effect of the cross-sectional area variation of the part on the heat transfer and flow characteristics of swirl cooling and obtain the optimal structure, cases 3 and 4 are conducted. A_a is the cross-sectional area of each part and *AR* is the ratio of the width *w* to the height *h*. The detailed cross-sectional area variation of the parts is presented in Table 1.

In order to analyze the local variation of the Nusselt number and pressure loss coefficient along the flow direction, 72 local planes are set and detailed location distributions are shown in Fig. 3.

2.2. Numerical method

The boundary conditions used in the simulations are presented in Table 2. The mainstream and coolant adopt ideal air and the inlet and outlet of the mainstream are set to pressure conditions. The inlet Reynolds number of the leading edge is kept unchanged during the simulations. The inlet Reynolds number of the mid-chord region varies from 12,000 to 52000. The outlets of the leading edge and mid-chord region are set to pressure conditions. The blade material is stainless steel. The material density and thermal conductivity are 8030 kg/m^3 and 16.27 W/(m·K), respectively. All the walls are set to non-slip boundary conditions. The endwall, blade tip and hub are adiabatic walls without thickness.

The commercial software ANSYS ICEM19.2 is adopted to generate unstructured meshes in the fluid and solid domains, as shown in Fig. 4. Prism grids are set at the interfaces between the fluid and solid regions. The commercial software ANSYS FLUENT19.2 is used to solve the Reynolds-Averaged Navier-Stokes equations and the Standard k-ε turbulent model with enhanced wall function. The SIMPLE scheme is adopted for the pressure–velocity coupling. The Least Squares Cell Based is applied to discretize the gradient and the Second Order Upwind is applied to discretize the pressure, density, momentum, turbulent kinetic energy, and turbulent dissipation rate.In order to obtain accurate numerical results, the root mean square residuals of the mass and momentum equations are less than 10^{-3} and that of the energy equation is less than 10^{-6}.

The results conducted by Ling et al. [34] are used for comparison to test the numerical results, as shown in Fig. 5. For the k-ω and *SST* turbulent models, $y+$ is lower than 1 and the growth factor for the cell is set
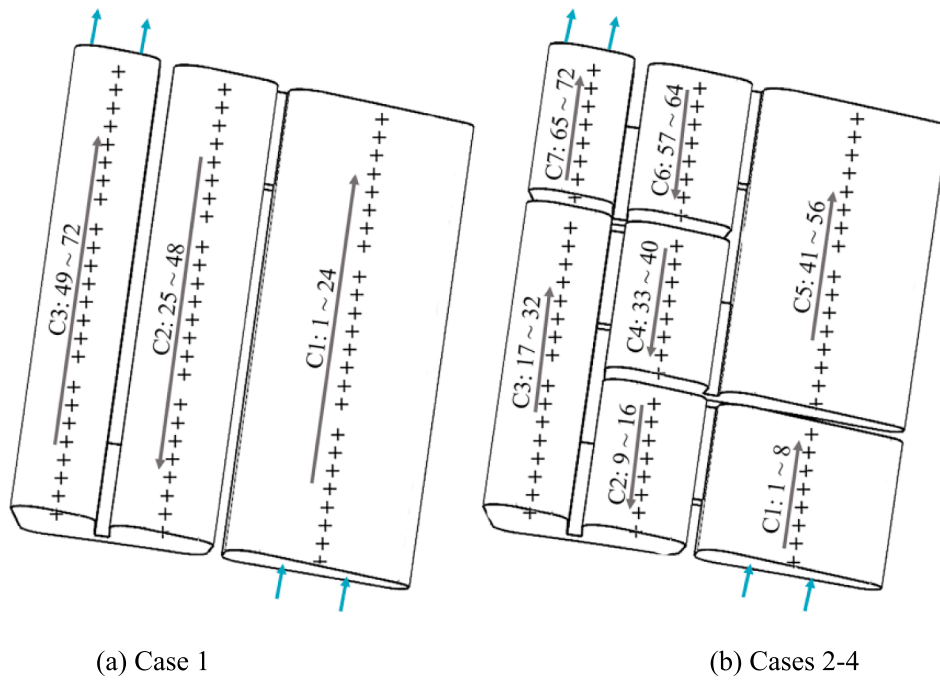
experimental data.

To sum up, the research on swirl cooling at the mid-chord region of the blade is limit at present. Furthermore, although the two-stage swirl cooling is adopted in Khalatov et al.'s study [33], the swirl channel is still too long that the maximum drop of Nusselt number is almost 60 % along the channel due to the viscous dissipation and swirl flow decay. Therefore, in this paper we shorten the swirl chamber further and propose seven-stage short chambers with six inject nozzles to form the multi-stage swirl cooling at the mid-chord region of the blade. The distributions of the velocities and temperatures in the chambers are studied. The effects of Reynolds numbers on the Nusselt number, pressure loss coefficient, and cooling effectiveness at the mid-chord region of the blade are obtained. The results of swirl cooling are also compared with those of enhanced convective heat transfer with ribs.

2. Geometry model and numerical method

2.1. Geometry structure

A NASA C3X turbine blade is chosen and the computational model is shown in Fig. 1. The chord length and height of the blade are 144.93 mm and 76.2 mm, respectively. The blade pitch is set to 117.73 mm.

In order to avoid the effect of the inlet and outlet on the computational results, the inlet and outlet channels are set to 1 and 1.5 times as length as the chord. The whole blade is divided into the two parts: the

(a) Case 1   (b) Cases 2-4

Fig. 3. Location information.

Table 2
Boundary conditions.

Location	Parameter	Value
Mainstream inlet	Total pressure (Pa)	305,793
	Total temperature (K)	701
	Turbulence intensity	5 %
Mainstream outlet	Outlet pressure (Pa)	215,328
Leading edge inlet	Reynolds number	25,989
	Total temperature (K)	450
Leading edge outlet	Outlet pressure (Pa)	200,000
Mid-chord inlet	Reynolds number	12000–52000
	Total temperature (K)	450
Mid-chord outlet	Outlet pressure (Pa)	200,000

as 1.2. For the Standard k-ε, Realized k-ε, and RNG k-ε turbulent models, $y+$ is lower than 11 and the growth factor for the cell is set as 1.2. It can be seen that Nusselt numbers obtained by using four turbulent models show almost the same trend compared with the experimental ones. However, Nusselt numbers obtained by using the k-ω and SST turbulent models are far lower than the experimental data. Nusselt numbers obtained by using the RNG k-ε turbulent model are higher at the first inlet nozzle. Nusselt numbers obtained using the Standard k-ε and Realized k-ε turbulent models show a little lower at the first inlet nozzle. The Standard k-ε turbulent model needs less converging time and therefore is chosen for current simulations.

The effects of the mesh number for case 2 are analyzed shown in Fig. 6. The external temperature distributions at 50 % blade height are adopted for comparison. When the value is above 18.68 million, the mesh number has no influence on the blade temperature and the results are reliable. For the four cases, the same method is chosen to generate
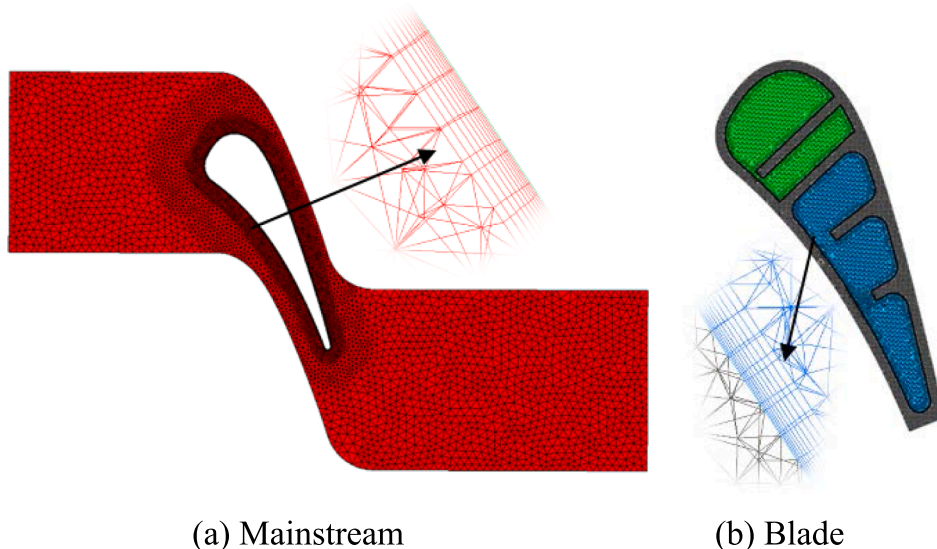

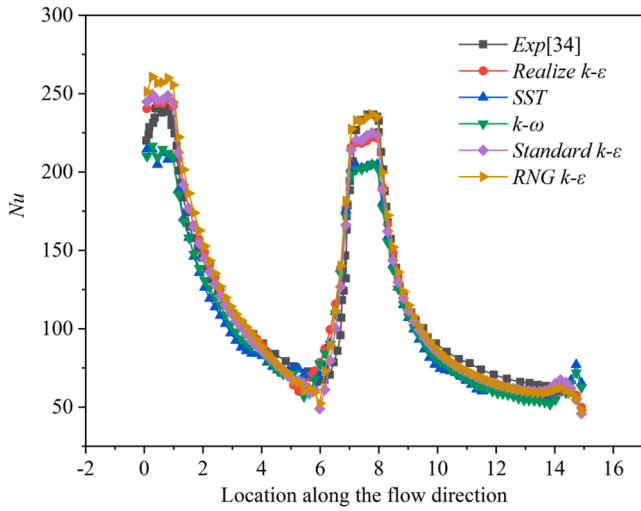(a) Mainstream   (b) Blade

Fig. 4. Mesh.

Fig. 5. Comparison of the Nusselt number using different turbulent models.
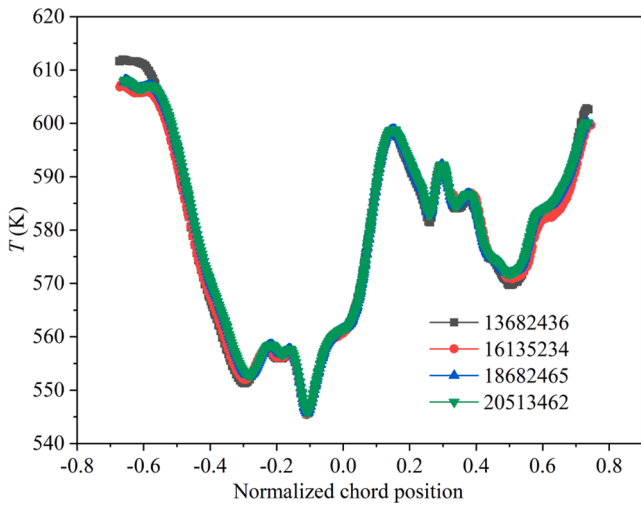

Fig. 6. The temperature distributions at the 50% blade height.

meshesand the mesh numbers are 18.31 million, 18.68 million, 18.43 million, and 18.97 million. The grid convergence index (GCI) method is employed to valid the current mesh independence by comparing the average Nusselt number [36]. GCI_{12} is 1.09 % which demonstrates that the mesh number with more than 18.68 million has no influence on the average Nusselt number. For other cases, GCI_{12} are 1.24 %, 1.18 %, and 1.01 %, respectively.

Reynolds number is defined as follows:

$$Re = \frac{\rho U D}{\mu} = \frac{\dot{m}D}{\mu A_a} \tag{1}$$

where ρ is the density, kg/m³; U is the velocity, m/s; D is the average hydraulic diameter of the cooling chambers, m; μ is the dynamic viscosity, Pa·s; $\dot{m}$ is the mass flow rate, kg/s ; A_a is the cross-sectional area of the chamber, m².

Nusselt number Nu is shown as follows:

$$Nu = \frac{qD}{(T_{wi} - T_b)\lambda} \tag{2}$$

where q is the average heat flux at the interface between the fluid and solid region, W/(m²•K); D is the hydraulic diameter of the cooling chambers, m; λ is the thermal conductivity of the coolant, W/(m·K); T_{wi} and T_b are the wall temperature and the coolant temperature, K;

Friction factor f is defined as follows:

$$f = \frac{2\Delta P D}{\rho U^2 L} \tag{3}$$

where L is the length of the swirl chamber, mm; ΔP is the pressure difference, Pa.

The comprehensive thermal performance j is calculated as follows:

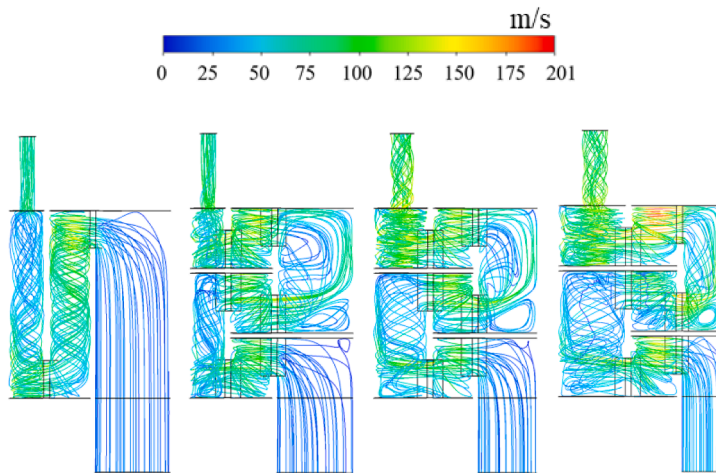$$j = \frac{Nu/Nu_\infty}{(f/f_\infty)^{1/3}} \tag{4}$$

where Nu_∞ and f_∞ are the Nusselt number and friction factor in the smooth tube [35].

$$Nu_\infty = \frac{f_\infty/8(Re - 1000)Pr}{1 + 12.7(f_\infty/8)^{1/2}(Pr^{2/3} - 1)} \tag{5}$$

$$f_\infty = (0.79\ln Re - 1.64)^{-2} \tag{6}$$

The pressure loss coefficient C_{Pt} is calculated as follows:

(a) Case 1   (b) Case 2   (c) Case 3   (d) Case 4

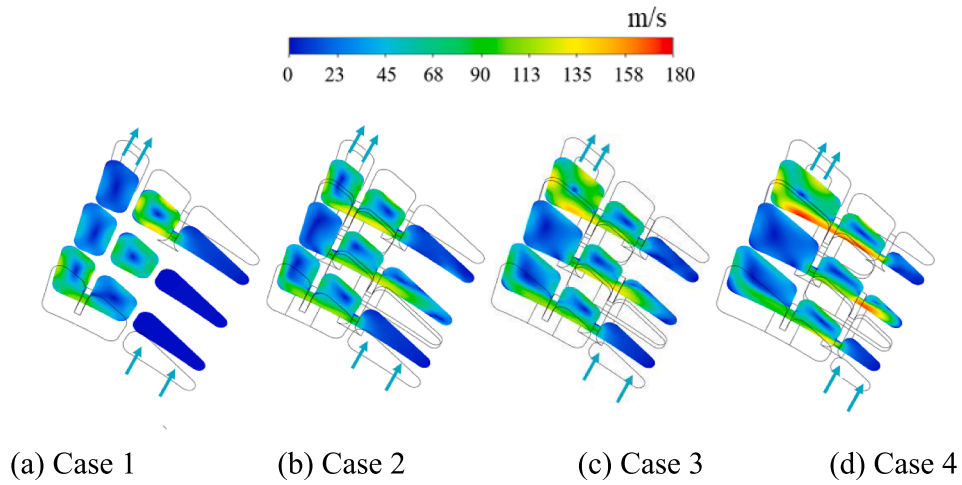**Fig. 7.** Streamline inside the chamber.

(a) Case 1 (b) Case 2 (c) Case 3 (d) Case 4

Fig. 8. The circumferential velocity contourat different locations.
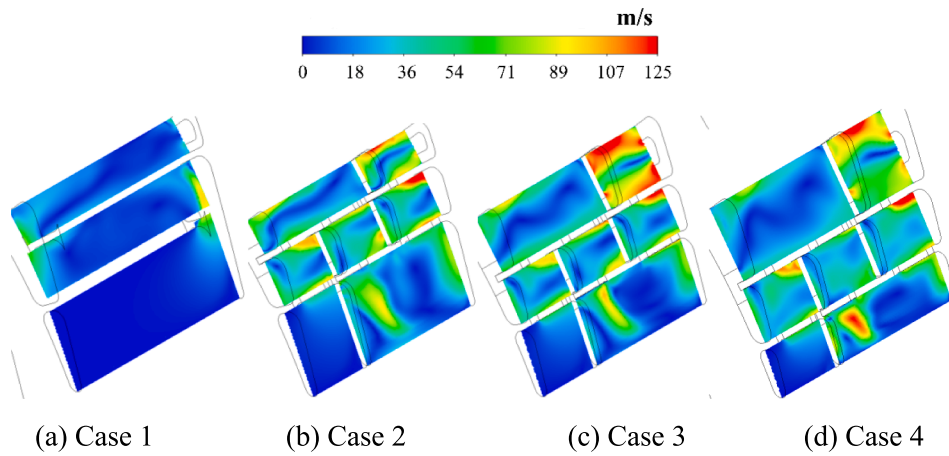

(a) Case 1 (b) Case 2 (c) Case 3 (d) Case 4

Fig. 9. The circumferential velocity contour at X-Z plane.

$$C_{Pt} = \frac{P_{in} - P}{P_{in}} \quad (7)$$

where P_{in} is the inlet pressure of the coolant, Pa; P is the local pressure of the coolant, Pa.

The cooling effectiveness η is defined as follows:

$$\eta = \frac{T_h - T_{wo}}{T_h - T_c} \quad (8)$$

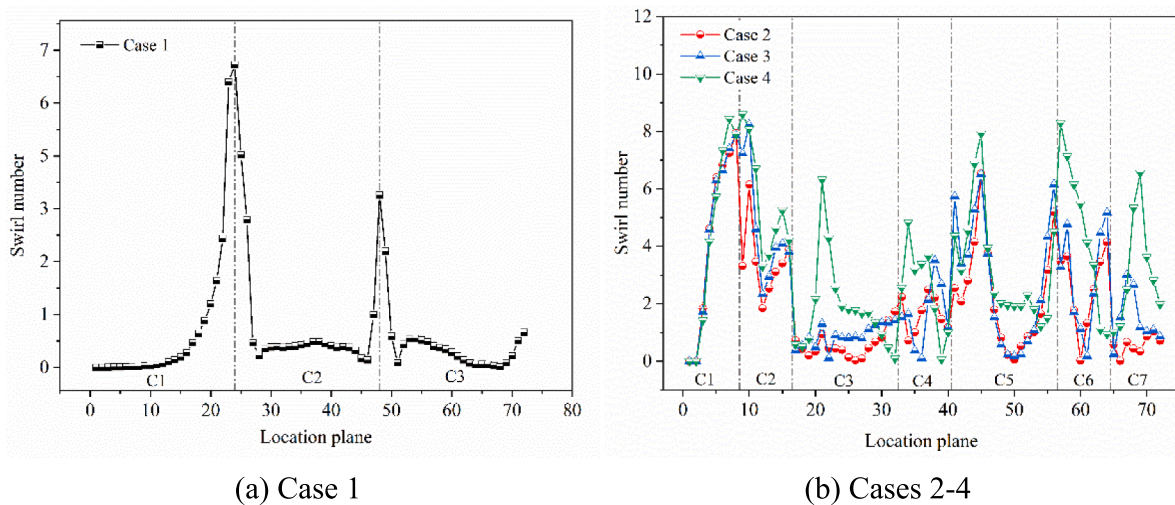where T_h is the mainstream inlet temperature, K; T_c is the coolant inlet

(a) Case 1 (b) Cases 2-4

Fig. 10. The circumferentially averaged swirl number.
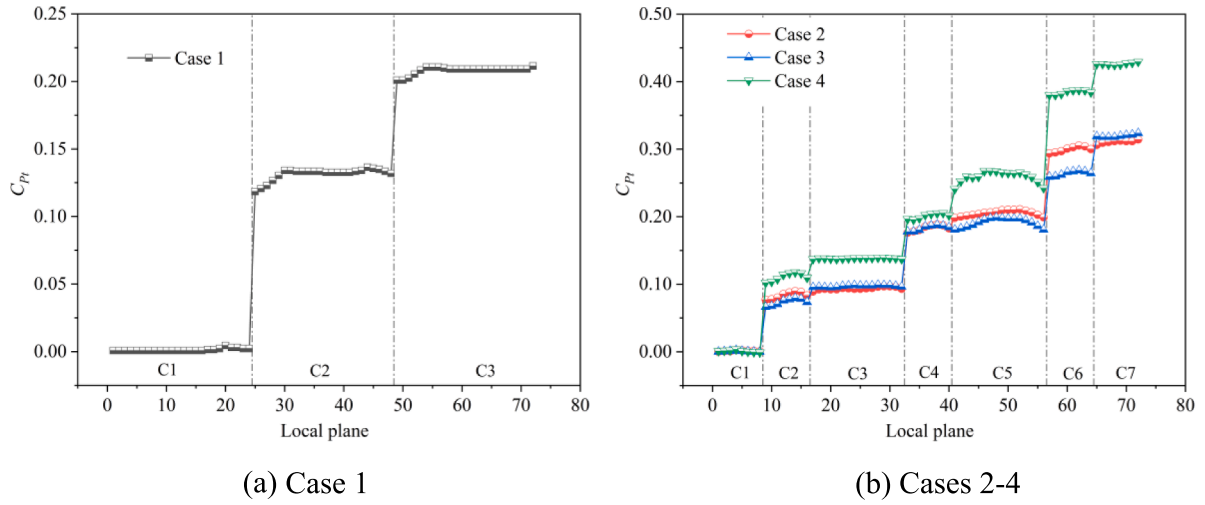
(a) Case 1 (b) Cases 2-4

Fig. 11. Local pressure loss coefficients.

temperature, K; T_{wo} is the external wall temperature of the blade, K.

The non-uniformity factor of the temperature σ is conducted as follows:

$$\sigma = \sqrt{\frac{\sum_{i=1}^{N}(T-\overline{T})^2}{N}} \tag{9}$$

The circumferentially averaged swirl number S is defined as follows:

$$S = \frac{\dot{I}_\varphi}{R\dot{I}_z} = \frac{\int_A \rho u_z u_\varphi r dA}{R\int_A \rho u_z^2 dA} \tag{10}$$

where $\dot{I}_\varphi$ and $\dot{I}_z$ are the averaged angular and axial momentum in different cross sections of the swirl chambers.

3. Results and discussion

3.1. Fluid flow and pressure drop

There are several swirl chambers in the present cases which make the fluid flow more complicated compared to the convectional swirl cooling structure. Therefore, in this part, the detailed streamline and contour distributions of the velocity of the coolant in four types of swirl structures are presented. The streamline and circumferential velocity of the

coolant are shown in Figs. 7-9 when the inlet Reynolds number is 31,900 for four cases. Three cross-sectional planes are located at 16 %, 50 %, and 84 % of the blade height in Fig. 8. Fig. 10 shows the circumferentially averaged swirl number along the chamber.

In the first chamber (C1) of case 1, the streamlines are distributed uniformly this is because the coolant flows into the chamber along the axial direction and therefore there is no circumferential velocity shown in Fig. 8(a) and 9(a). When the coolant flows through the swirl nozzles which connect two adjacent chambers, the swirl flow is formed and higher swirl numbers are achieved near the top and bottom locations of the blade shown in Fig. 10(a). This is because the axial components of the flow are restricted at these locations. However, the circumferential velocities and swirl numbers decrease remarkably along the flow direction in *C*2 and C3 due to the viscous dissipation and swirl flow decay in the long chambers. Therefore, for cases 2–4, the chambers are separated into seven short ones to keep high swirl intensity. It is obvious that the whole swirl intensities are improved. For the short chambers, such as, *C*2, C4, C6, and C7, the flow is disturbed continually and therefore the boundary layers are destroyed due to the proximity of the inlet nozzle to the outlet one. The phenomenon that the swirl numbers shown in Fig. 10(b) are quite high near these regions also demonstrates this point. Fig. 9(b-d) present that the swirl axes in cases 2–4 are not directly in the chamber center but follow a wave-like trend. This phenomenon is due to the effect of the non-symmetry inlet nozzles, which is also
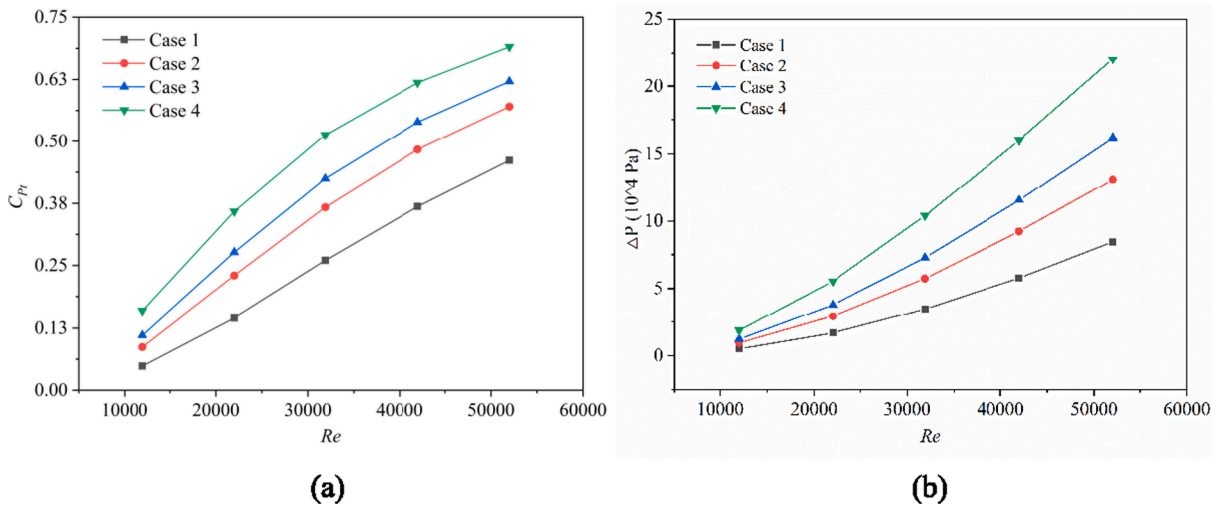

(a) (b)

Fig. 12. Total pressure loss coefficient and pressure drops under different Reynolds numbers.

(a) Case 1   (b) Case 2
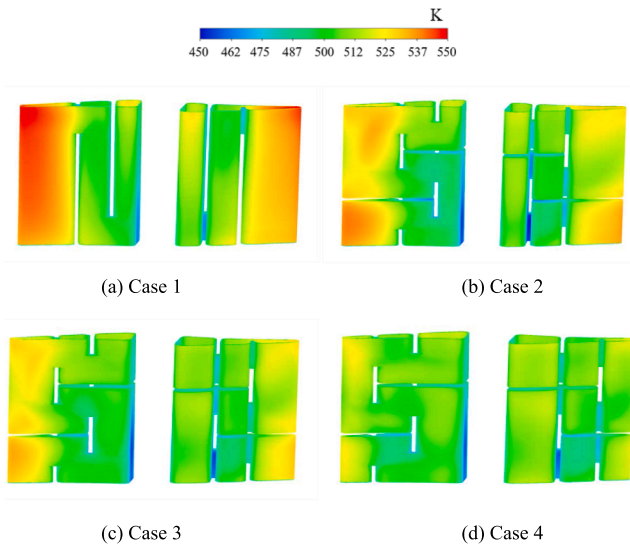
(c) Case 3   (d) Case 4

Fig. 13. Temperature distributions of the internal surface at the mid-chord region.

observed in the previous studies [9,31]. This type of the circumferential flow is defined as a solid-body vortex, which is proved to be a more desirable topology for heat transfer. However, C3 and C5 are still a little longer and should be shortened in the future. The ratio of width to height AR in part C for case 2 is 0.59 presented in Table 2 and increased to 0.98 and 1.28, respectively for cases 3 and 4. For part B, AR is increased from 1.08 for case 2 to 1.23 and 1.61 for cases 3 and 4, respectively. These adjustments lead to the obviously improved swirl numbers in parts B and C. Therefore, it can be concluded that in order to achieve higher swirl number the width of the chamber should be larger than the height.

Fig. 11 shows the local pressure loss coefficients along the flow direction for four cases. In C1, there is no jet nozzle and therefore the pressure loss coefficient keeps low value. In other chambers, although exist of the jet nozzle could induce the swirl flow, it is inevitable to increase the pressure loss coefficient due to the throttling effect. In addition, the coolant flows in a reverse direction after passing through the jet nozzles, which also makes a contribution to the increase of the pressure loss coefficient. However, in each swirl chamber, the pressure loss coefficient could be kept almost unchanged, except near the inlet and outlet of the chamber. Therefore, the pressure loss coefficients for all

cases present a ladder-type growth. Based on the above results, it can be concluded that optimizing the jet nozzle and avoiding the change of flow direction may be two of the effective ways to reduce the pressure drop of the swirl cooling.

The total pressure loss coefficients and pressure drops with different Reynolds numbers for four cases are shown in Fig. 12. It is well known that the pressure drops are increased with the Reynolds numbers. Based on the above analysis, case 1 only has two jet nozzles and the flow direction is changed two times. Therefore the pressure loss coefficient is the lowest. For other cases, the increase of the jet nozzle number and flow turns number both lead to the increase of pressure loss coefficient. Case 4 shows the highest pressure loss coefficient because the smallest inlet cross-sectional area is set and therefore the inlet velocity is the highest under the same Reynolds number. As shown in Fig. 12(b), the increase rate of the total pressure drop for case 4 is higher than those for other cases. When Re is 12000, the total pressure drop is 18.65 kPa, which is increased by 270.48 %, 99.08 %, and 52.49 %, respectively compared with that for cases 1–3. When Re is incease to 52000, the total pressure drop is 220.2 kPa, which is increased by 160.72 %, 68.22 %, and 26.57 %, respectively.

3.2. Temperature distributions and heat transfer of the internal surface

In this section, temperature distributions and heat transfer characteristics of the coolant on the internal surface of the mid-chord region of the blade are analyzed and the local and averaged Nusselt numbers under different Reynolds numbers are presented.

Temperature distributions on the internal surface of the mid-chord region of the blade are shown in Fig. 13. As shown in Fig. 13(a), the temperatures on the surface of C1 are obviously higher than those of $C2$ and C3. This is because the convective flow in C1 has lower heat transfer coefficient. When the coolant flows into $C2$ and C3, the swirl flow is formed and heat transfer capability is improved. It also can be seen that at the end of the chamber, the temperature is a little higher due to the gradual reduction of the swirl velocity along the axial direction. For case 2, the surfaces of C1 and C5 both show higher temperatures. The reason is that the flow in C1 is convective heat transfer and the heat transfer capability is not as high as swirl cooling. C5 has large AR and is hard to form the swirl flow. Therefore, the circumferential velocity is low shown in Fig. 8(b). Through adjusting the cross-sectional areas of three parts at the mid-chord region of the blade, the velocities of the coolant in C1 and C5 are increased and therefore the surface temperatures are reduced remarkably shown in cases 3 and 4. In conclusion, all chamber surfaces in case 4 show lower temperatures compared with other cases and the cross-sectional area distributions of three parts at the mid-chord region
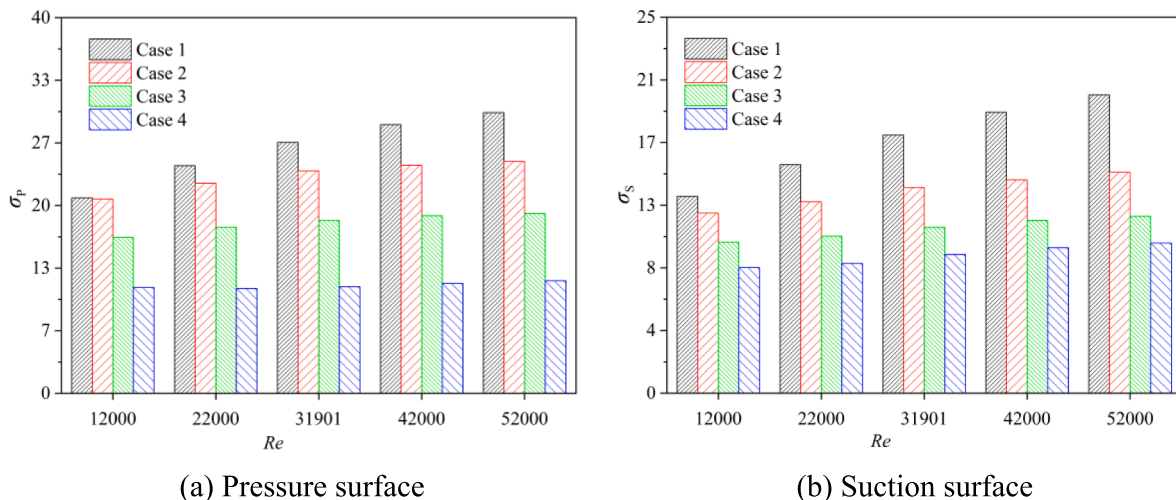

(a) Pressure surface   (b) Suction surface

Fig. 14. The non-uniformity factor of the temperatures.

(a) Case 1   (b) Cases 2-4
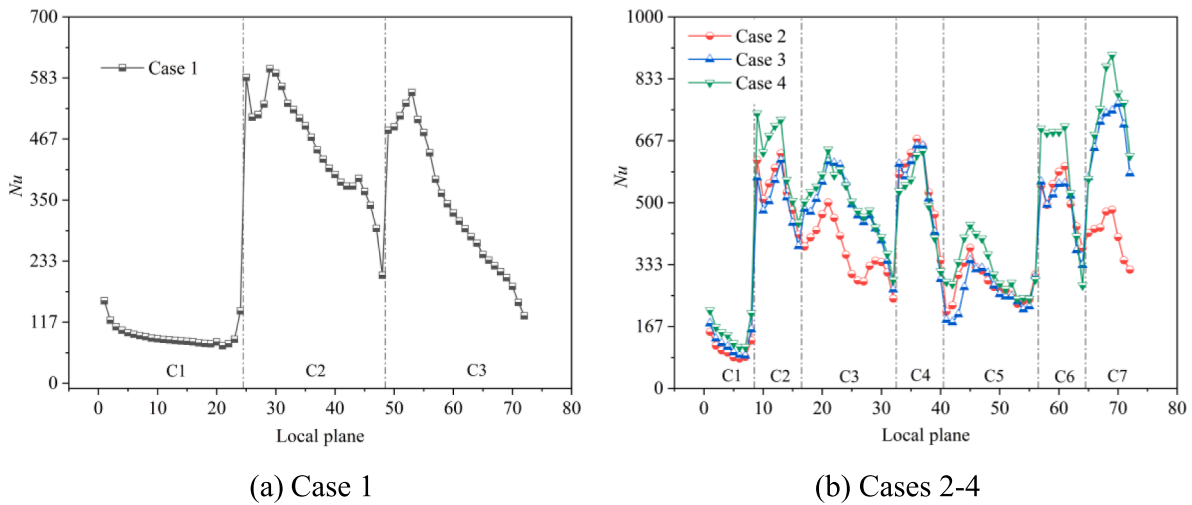
Fig. 15. Local Nusselt number distributions.
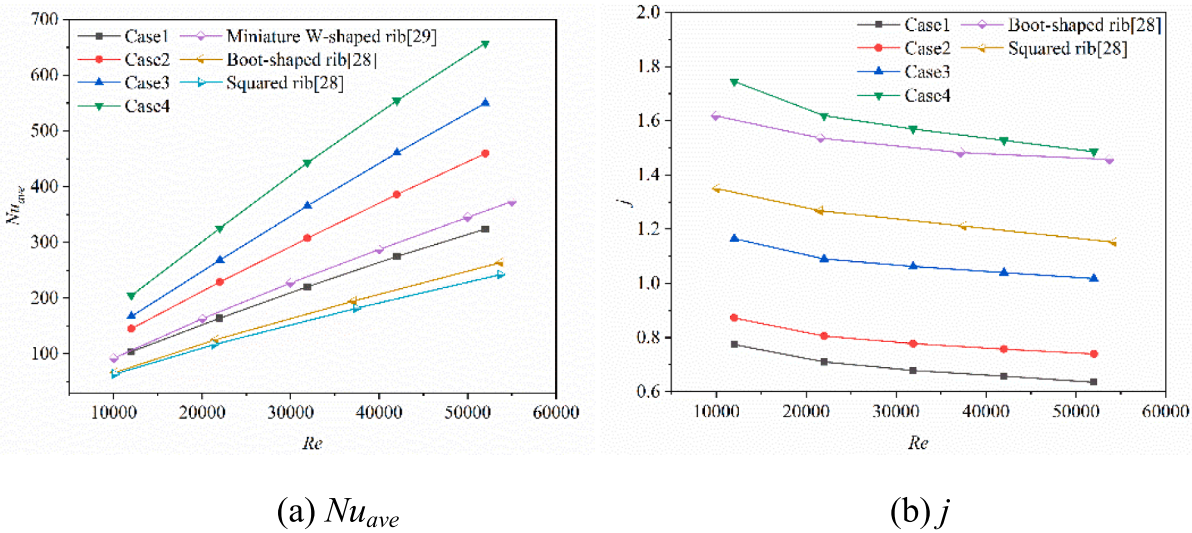

(a) Nu_{ave} (b) j

Fig. 16. Averaged Nusselt number and comprehensive thermal performance.

of the blade is optimal.

During the blade cooling process, if the temperature gradient on the blade surface is too high, the thermal fatigue will occur and this phenomenon also could lead to the failure of the blade. Therefore, the non-uniformity factor of the blade surface temperature is one of the key parameters to evaluate a cooling technique.

Fig. 14 shows the non-uniformity factor of the external surface temperature at the mid-chord region of the blade. It can be seen when the mid-chord region of the blade is divided into more chambers, the temperature distributions on the external surface are more uniform. Furthermore, with increasing the Reynolds number, the non-uniformity factor of the temperature for case 1 is increased by 43.58 %-51.49 %. However, Reynolds number has not that much effect on the non-uniformity factor of the temperature for case 4, which are increased only by 19.52 % on the suction surface and 6.21 % on the pressure surface.

Fig. 15 shows the distributions of the local Nusselt number of the internal surface at the mid-chord region of the blade along the flow direction. The Nusselt number at the inlet location of C1 shows higher value due to the entrance effect and decreases gradually along the flow direction. It can be seen that for each case the Nusselt numbers in C1 are obviously lower than those in other chambers, which demonstrates that

the heat transfer capability of swirl flow is much higher than the convective flow. After flowing through the jet nozzle, the Nusselt number is improved remarkably. However, the Nusselt number is decreased obviously along the flow direction due to the reduction of the swirl velocity. As shown in Fig. 15(b), the Nusselt numbers of C3 and C7 in case 3 and 4 are higher than those in case 2, which demonstrates that the increase of the cross-sectional area of part C has positive effect on the heat transfer performance of the coolant.

With increasing the Reynolds numbers, it is no doubt that averaged Nusselt numbers Nu_{ave} for each case are increased, as shown in Fig. 16 (a). Compared with the three-stage one in case 1, the seven-stage swirl cooling structure in cases 2–4 performs higher Nu_{ave}. For example, when the Reynolds number varies from 12,000 to 52000, Nu_{ave} in case 4 is increased by 57.23 %-64.12 % compared with that in case 1. It can be concluded that the cooling structure adopted in case 4 shows the best heat transfer capability for the current study. At the same time, the pressure drop in case 4 is the highest among these cases. Therefore, in order to consider the combined effect of the heat transfer and pressure loss, the comprehensive thermal performance j is employed. As shown in Fig. 16(b), j is decreased with increasing the Reynolds number. It also can be seen that case 4 shows the best performance on j. Compared with that in case 1, j in case 4 is improved by 81.32 %-87.62 %.
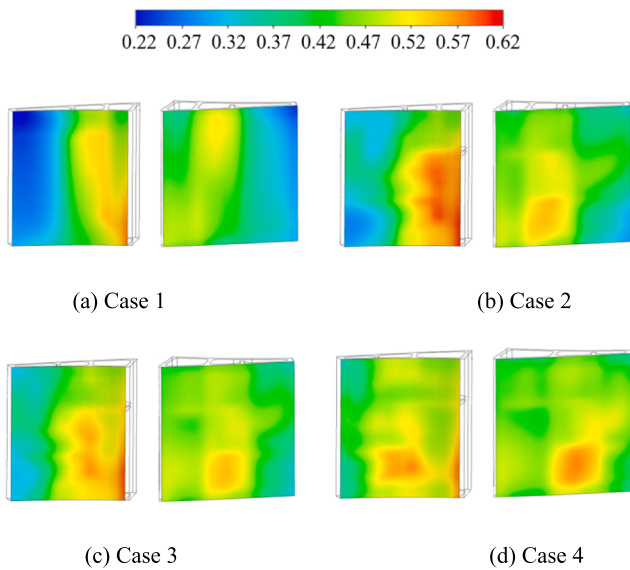
(a) Case 1   (b) Case 2

(c) Case 3   (d) Case 4

Fig. 17. Cooling effectiveness on the external surface of the blade.

The results of the multi-stage swirl cooling in this study are compared with the enhanced convective heat transfer with squared, boot-shaped, and miniature w-shaped ribs [28,29]. As shown in Fig. 16 (a), the seven-stage swirl cooling structures in cases 2–4 show higher Nu_{ave} than the enhanced convective heat transfer with various ribs. Due to the higher pressure drops, the comprehensive thermal performances for cases 2 and 3 are lower than those obtained by the enhanced convective heat transfer with various ribs shown in Fig. 16(b). However, the highest j is achieved in case 4.

3.3. Cooling effectiveness

The cooling effectiveness is a meaningful parameter which demonstrates the coupled fluid–solid-thermal interaction between the mainstream, the coolant, and the blade. Fig. 17 shows the cooling effectiveness contour on the external surface of the blade. For case 1, the heat transfer capability in C1 is rather weak and so is the cooling effectiveness. However, in $C2$ and C3 the swirl flow is formed and heat transfer capability is obviously improved. Therefore, the cooling effectiveness in these chambers is enhanced remarkably. Although the chamber is divided into seven short ones, the cooling effectiveness in

part A is still low for case 2 because the chambers in part A are not suitable to form the swirl flow and the surface temperatures are high. However, the pressure surfaces of C2-4 present higher cooling effectiveness than other surfaces. Through adjusting the chamber structures, the whole surfaces in cases 3 and 4 show the high cooling effectiveness, which is above 0.32.

Fig. 18 shows the effect of the Reynolds number on the averaged cooling effectiveness η_{ave} on the external surfaces of the blade. The seven-stage swirl structure in cases 2–4 shows higher cooling effectiveness compared with the three-stage one in case 1, especially at high Reynolds number. When the Reynolds number varies from 12,000 to 52000, η_{ave} in case 4 is increased by 16.38 %-21.63 % on the pressure surface and 10.48 %-16.27 % on the suction surface compared with those in case 1.

4. Conclusions

In this paper, four types of the multi-stage swirl chamber models are adopted at the mid-chord region of the gas turbine blade. Detailed investigations on flow and heat transfer characteristics of the cooling air in these chambers are conducted. The coupled fluid–solid-thermal interaction between the mainstream, the cooling air, and the blade is studied numerically. The results show that the circumferential velocity in the long chambers of case 1 is reduced gradually along the axial direction and so is the swirl number due to the viscous dissipation and swirl flow decay. Therefore, the Nusselt number is decreased obviously. After shortening the swirl chambers in cases 2–4, the circumferential velocity and swirl number could keep high value which leads to the higher Nusselt number. However, the total pressure drops are increased remarkably due to the increase of jet nozzles and number of flow turns. Even so, the comprehensive thermal performance is still enhanced because the Nusselt number is also increased remarkably. For cases 2–4, the ratios of width to height for parts B and C are increased from 0.59 and 1.08 to 1.28 and 1.61, respectively. The obviously improved swirl numbers in parts B and C are achieved through these adjustments, which leads to higher averaged Nusselt number and cooling effectiveness. Compared with the enhanced convective heat transfer with various ribs, the multi-stage swirl cooling method in case 4 shows better comprehensive thermal performance.

Based on the current study, it is suggested that optimizing the jet nozzle structure and reducing the number of flow turn are two of the effective ways to improve the comprehensive thermal performance of the swirl cooling. Because the throttling effect of the swirl nozzle and the flow turn could increase the pressure drop remarkably. In addition, the
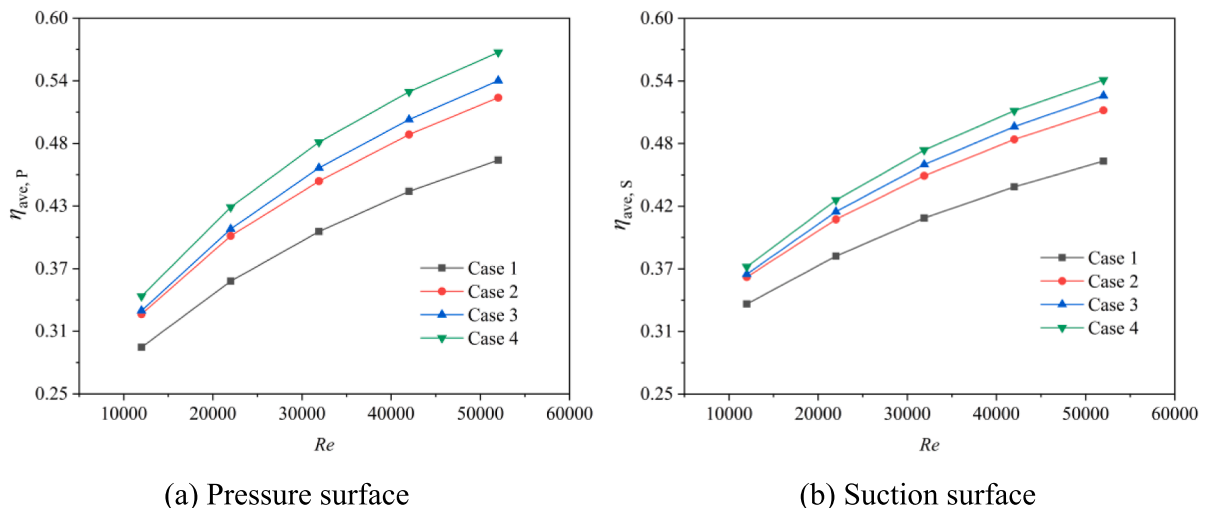

(a) Pressure surface   (b) Suction surface

Fig. 18. Averaged cooling effectiveness with Reynolds number.

cross-sectional width should be equal to or large than the cross-sectional height for parts B and C to increase the swirl intensity. At last, the lower Reynolds number should be employed because the comprehensive thermal performance is decreased with the Reynolds number.

Declaration of Competing Interest

The authors declare that they have no known competing financial interests or personal relationships that could have appeared to influence the work reported in this paper.

Data availability

Data will be made available on request.

Acknowledgement

References

[1] J.C. Han, S. Dutta, S. Ekkad, Gas turbine heat transfer and cooling technology, CRC Press (2012) 1.

[2] F. Kreith, D. Margolis, Heat transfer and friction in turbulent vortex flow, Applied Scientific Research 8 (1959) 457–473.

[3] N. Hay, P.D. West, Heat transfer in free swirling flow in a pipe, Journal of Heat Transfer 97 (3) (1975) 411–416.

[4] P.M. Ligrani, M.M. Oliveira, T. Blaskovich, Comparison of heat transfer augmentation techniques, AIAA Journal 41)(3 (2003) 337–362.

[5] B. Glezer, H.K. Moon, T. O'Connell. A novel technique for the internal blade cooling. Presented at the International Gas Turbine and Aeroengine Congress & Exhibition Birmingham, UK, June 10-13, 1996.

[6] C.R. Hedlund, P.M. Ligrani, H.K. Moon, B. Glezer, Heat transfer and flow phenomena in a swirl chamber simulating turbine blade internal cooling, Journal of Turbomachinery 121 (1999) 804–813.

[7] C.R. Hedlund, P.M. Ligrani, Local swirl chamber heat transfer and flow structure at different Reynolds numbers, Journal of Turbomachinery 122 (2000) 375–385.

[8] C. Biegger, B. Weigand, Flow and heat transfer measurements in a swirl chamber with different outlet geometries, Experimental fluids 56 (2015) 78.

[9] C. Biegger, Y. Rao, B. Weigand, Flow and heat transfer measurements in swirl tubes with one and multiple tangential inlet jets for internal gas turbine blade cooling, International Journal of Heat and Fluid flow 73 (2018) 174–187.

[10] X. Fan, L. Li, J. Zou, J. Wang, F. Wu, Local heat transfer of vortex cooling with multiple tangential nozzles in a gas turbine blade leading edge cooling passage, International Journal of Heat and Mass Transfer 126 (2018) 377–389.

[11] X. Fan, C. He, L. Gan, L. Li, C. Du, Experimental study of swirling flow characteristics in a semi cylinder vortex cooling configuration, Experimental Thermal and Fluid Science 113 (2020) 110036.

[12] H. Fawzy, Q. Zheng, N. Ahmad, Effect of slot area ratio and slot angle on swirl cooling in a gas turbine blade leading edge, Journal of Aerospace Engineering 33 (5) (2020) 04020046.

[13] H. Fawzy, Q. Zheng, N. Ahmad, Y. Jiang, Optimization of a swirl with impingement compound cooling unit for a gas turbine blade leading edge, Energies 13 (1) (2020) 210.

[14] S.M. Mousavi, B. Ghadimi, F. Kowsary, Numerical study on the effects of multiple inlet slot configurations on swirl cooling of a gas turbine blade leading edge, International Communications in Heat and Mass Transfer 90 (2018) 34–43.

[15] X. Fan, L. Li, J. Zou, Y. Zhou, Cooling methods for gas turbine blade leading edge: comparative study on impingment cooling, vortex cooling and double vortex cooling, International Communications in Heat and Mass Transfer 100 (2019) 133–145.

[16] X. Fan, Y. Xue, Numerical investigation of nozzle geometry influence on the vortex cooling in an actual gas turbine blade leading edge cooling system, Heat and Mass Transfer 58 (2022) 575–586.

[17] J. Wang, C. Du, F. Wu, L. Li, X. Fan, Investigation of the vortex cooling flow and heat transfer behavior in variable cross-section vortex chambers for gas turbine blade leading edge, International Communications in Heat and Mass Transfer 108 (2019), 104301.

[18] H. Li, Y. Gao, C. Du, W. Hong, Numerical study on swirl cooling flow, heat transfer and stress characteristics based on fluid-structure coupling method under different swirl chamber heights and Reynolds numbers, International Journal of Heat and Mass Transfer 173 (2021) 121228.

[19] Y. Liu, Y. Rao, B. Weigand, Heat transfer and pressure loss characteristics in a swirl cooling tube with dimples on the tube inner surface, Journal of Heat and Mass Transfer 128 (2019) 54–65.

[20] H.M. Alhajeri, A. Almutairi, A.H. Alenezi, A.A.A. Gamil, Numerical investigation on heat transfer performance and flow characteristics in a roughed vortex chamber, Applied Thermal Engineering 153 (2019) 58–68.

[21] H. Du, Z. Mei, J. Zou, W. Jiang, D. Xie, Conjugate heat transfer investigation on swirl-film cooling at the leading edge of a gas turbine vane, Entropy 21 (2019) 1007.

[22] R. Hou, F. Wen, Y. Luo, S. Wang, Influence of inlet swirl on film cooling of the turbine leading edge, Heat Transfer Engineering 42 (12) (2021) 985–1001.

[23] N. Wang, J. Han, Swirl impinging cooling on an airfoil leading edge model at large Reynolds number, Journal of Thermal Science and Engineering Applications 11 (3) (2019), 031006.

[24] J. Zhou, X. Wang, J. Li, W. Hou, Comparison between impingement/effusion and double swirl/effusion cooling performance under different effusion hole diameters, International Journal of Heat and Mass Transfer 141 (2019) 1097–1113.

[25] J. Wang, L. Li, J. Li, F. Wu, C. Du, Numerical investigation on flow and heat transfer characteristics of vortex cooling in an actual film-cooled leading edge, Applied Thermal Engineering 185 (2021), 115942.

[26] R. Yao, H. Su, Y. Cheng, J. Wang, J. Pu, Numerical investigation of a novel multistage swirl cooling conception in blade leading edge of gas turbine, International Journal of Thermal Sciences 172 (2022), 107269.

[27] K. Xiao, J. He, Z. Feng, Study on flow and heat transfer characteristics of a new-proposed alternating elliptical U-channel in the midchord region of gas turbine blade, Journal of Engineering for Gas Turbines and Power 143 (2021) 051025.

[28] K. Pham, Q. Nguyen, T. Vu, C. Dinh, Effects of boot-shaped rib on heat transfer characteristics of internal cooling turbine blades, Journal of Heat Transfer 142 (2020), 102106.

[29] Y. Rao, Z. Guo, D. Wang, Experimental and numerical study of heat transfer and turbulent flow characteristics in three-short-pass serpentine cooling channel with miniature w-ribs, Journal of Heat Transfer 142 (2020), 121901.

[30] R.S. Amano, A.R. Salem, F.N. Nourin, M. Abousabae, Experimental and numerical study of jet impingement cooling for improved gas turbine blade internal cooling with in-line and staggered nozzle arrays, Journal of Energy Resources Technology 143 (2021), 012103.

[31] M. Bruschewski, C. Scherhag, H.P. Schiffer, S. Grundmann, Influence of Channel Geometry and Flow Variables on Cyclone Cooling of Turbine Blades, Journal of Turbomachinery 138 (6) (2016), 061005.

[32] M. Bruschewski, S. Grundmann, H.P. Schiffer, Considerations for the design of swirl chambers for the cyclone cooling of turbine blades and for other applications with high swirl intensity, International Journal of Heat and Fluid Flow 86 (2020), 108670.

[33] A. Khalatov, N. Syred, P. Bowen, R. Al-Ajmi, A. Kozlov, A. Schukin. Innovative Cyclone Cooling Scheme for Gas Turbine Blade: Thermal-Hydraulic Performance Evaluation. Proceedings of ASME Turbo Expo 2000, Munich Germany, May 8-11, 2000.

[34] J.P.C.W. Ling, P.T. Ireland, N.W. Harvey. Measurement of Heat Transfer Coefficient Distributions and Flow Field in a Model of a Turbine Blade Cooling Passage with Tangential Injection. ASME Turbo Expo: Power for Land, Sea and Air, Barcelona, Spain, May 8-11, 2006.

[35] V. Gnielinski, New equations for heat and mass transfer in turbulent pipe and channel flow, International Chemical Engineering 16 (1976) 359–368.

[36] P.J. Roache, Perspective: A method for uniform reporting of grid refinement studies, Journal of Fluids Engineering 116 (1994) 405–413.